IEEE Access
Multidisciplinary | Rapid Review | Open Access Journal

Received September 16, 2020, accepted October 11, 2020, date of publication October 14, 2020, date of current version January 13, 2021.

Digital Object Identifier 10.1109/ACCESS.2020.3031091

Parameterized Local Maximum Synchrosqueezing Transform and Its Application in Engineering Vibration Signal Processing

ZHENFENG HUANG, DAHUAN WEI, ZHIWEI HUANG, HANLING MAO, XINXIN LI, RUI HUANG, AND PENGWEI XU

School of Mechanical Engineering, Guangxi University, Nanning 530004, China

Corresponding author: Hanling Mao (maohl79@gxu.edu.cn)

This work was supported in part by the Science and Technology Base and Talents Special Project of Guangxi Province under Grant AD19259002, in part by the Natural Science Foundation of Guangxi under Grant 2018GXNSFAA180116, Grant 2016GXNSFAA380119, and Grant 2018GXNSFAA138206, and in part by the National Natural Science Foundation of China under Grant 51365006.

ABSTRACT The time-frequency (TF) analysis (TFA) method is an effective tool for analyzing the time-variant features of non-stationary signals. Synchrosqueezing transform (SST) is a promising TFA method that has recently shown its usefulness in a wide range of engineering signal processing applications. On the other hand, the SST method suffers from some drawbacks, one of which is that when processing the frequency-modulated (FM) signal, the TF representation will smear heavily, which hinders its application in engineering vibration signals. In this paper, we propose a new TFA method named parameterized local maximum synchrosqueezing transform (PLMSST) to study engineering vibration signals with FM characteristics. First, the limitation of SST in signal processing is discussed. Next, we demodulate the signal by parameterizing the short-time Fourier transform (STFT) to correct the deviation of instantaneous frequency (IF) estimation. Further, we detect the local maximum of the spectrogram in the frequency direction to get the accurate IF estimate, and then obtain the energy-concentrated TF representation. Finally, we introduce the reconstruction function of this method. The performance of the proposed method is validated by both the numerical and experimental signals including vibration signals of the rolling bearing and the bridge. The results show that the proposed method is more effective in processing engineering vibration signals than other TFA methods.

INDEX TERMS Engineering vibration signal, frequency modulation, instantaneous frequency, synchrosqueezing transform, time-frequency analysis.

I. INTRODUCTION

Extracting dynamic features from complex engineering vibration signals is an effective way to study the state and inherent properties of structures. Vibration signals are usually non-stationary and nonlinear. The time-frequency (TF) analysis (TFA) method is one of the most popular and effective methods to deal with vibration signals because the TFA method can not only show the frequency information of signals but also reflect the law of frequency changing with time. The energy of signals will be concentrated at the instantaneous frequency (IF) of the TF plane and around it, so the IF can be obtained, and then the features of non-stationary signals can be extracted. Therefore, to accurately estimate the IF of vibration signals, it is indispensable to obtain the TF representation with high TF resolution.

Classical linear TFA methods, such as short-time Fourier transform (STFT) and wavelet transform, are often suffering from low TF resolution due to the limitation of the Heisenberg uncertainty principle. Bilinear TFA methods, such as Wigner-Ville distribution, can improve the TF resolution. But when processing multi-component signals, interference terms will be introduced. To improve the performance of TFA methods, Auger and Flandrin [1] proposed the TF reassignment method, which collects TF energy near the IF of the signal and improves the readability of the TF result. Since the reassignment method reassigns the TF Spectrogram into the IF trajectory along the two-dimensional (2-D) TF direction,

The associate editor coordinating the review of this manuscript and approving it for publication was Chih-Yu Hsu.

it loses the ability to reconstruct signals. Daubechies *et al.* [2] proposed synchrosqueezing transform (SST), which squeezes the TF coefficients into the IF trajectory only in the frequency direction and supports signal reconstruction. Thus, it is widely applied in various fields, such as electrocardiogram signals [3], acoustic signals [4], seismic signals [5], and mechanical signals [6], etc. When processing slowly varying signals, the result of SST is equivalent to the ideal TF representation. However, when the signals to be processed are frequency-modulated (FM) signals accompanied by noise, the TF representation of original TFA methods smear heavily. As a post-processing method, SST also suffers from low TF resolution [7], [8].

Many studies have recognized this drawback and put forward many improved methods. Li and Liang [9] used the demodulated operator to transform the time-variant frequency into a constant frequency, and then obtained a better TF resolution using SST. In order to address the multi-component and time-variant frequency signals, Feng *et al.* [10] decomposed each FM component with the generalized demodulation method, the IF of each mono-component being accurately estimated via SST. Wang *et al.* [11]–[13] proposed matching SST, further emerging into improved SST to enhance the energy concentration for the strong FM signals. Demodulation has been considered as an effective method to enhance the performance of the original SST [14]. However, the above-demodulated methods require the precise time-varying FM law. It should be noted that in most practical situations it is difficult to determine demodulated parameters precisely, especially for dealing with the noisy multi-component FM signals. In addition, due to the limitation of SST, these matching SST methods can only correct the deviation of IF estimation to a certain extent, and can not greatly improve the energy concentration of the TF representation.

Besides, second-order SST [15], [16], and high-order SST [17], [18] have been proposed, which greatly improve the energy concentration of the TF result. However, increasing the SST order will bring higher calculational cost and be easily disturbed by noise. Tu *et al.* [19] proposed a two-step algorithm, demodulated transform and high-order synchrosqueezing method to achieve a compact TF representation. Although obtaining better performance in FM signals, this method requires more computational cost than high-order SST. Yu [20] proposed synchroextracting transform (SET), which improves the readability of the TF result obviously. However, it could not achieve perfect signal reconstruction, which will lead to large reconstruction errors when processing strong FM signals. Zhu *et al.* [21] proposed synchroextracting chirplet transform to improve the accuracy of IF estimation. The TFA algorithm [22] combined polynomial chirplet transform and synchroextracting (PSE) was proposed, which can enhance the energy concentration of the TF representation of the strong FM signal. However, the method combined chirplet transform and synchroextracting is difficult to overcome the shortcoming of SET, i.e., achieving perfect reconstruction signal. Yu *et al.* [23] proposed multisynchrosqueezing transform, employing an iterative reassignment procedure to concentrate the blurry TF energy in a stepwise manner, meanwhile retaining the ability of signal reconstruction. Zhu *et al.* [24] proposed multisynchrosqueezing chirplet transform (MSSCT), which is considered to be a combination of adaptive chirplet transform and multisynchrosqueezing transform. Although these methods squeeze the TF coefficients into the ridge by applying multiple SST operations to improve the energy concentration of the TF result, they usually generate the IF trajectories that deviate from the true TF ridges when faced with the FM signals with noise, making it difficult to obtain a good TF representation.

The engineering vibration signal is the typical FM signal and often accompanied by background noise. A TFA method used to analyze engineering vibration signals should aim at 1) accurately estimating IF, 2) obtaining the high-resolution TF representation, and 3) allowing for perfect signal reconstruction. Therefore, in this paper, we propose a new TFA method, which uses two strategies: 1) parameterized TFA and 2) local maximum TF reassignment. In this way, the problem of IF bias estimation caused by noise interference in FM signals is solved, which does not need the precise time-varying FM law. With local maximum TF reassignment, the energy concentration of the TF representation can be improved to the greatest extent, and the influence of noise is small. In addition, perfect signal reconstruction can be realized.

II. SST

We begin this study with the framework of STFT. The expression of STFT-based SST can be written as

$$Ts(t,\omega') = \int_{-\infty}^{+\infty} G(t,\omega)\delta(\omega' - \omega_0(t,\omega))d\omega \tag{1}$$

where $G(t,\omega)$ is the STFT of signal $s(t)$, and the expression is as follows

$$G(t,\omega) = \int_{-\infty}^{+\infty} g(u-t)\cdot s(u)\cdot e^{-i\omega u}du \tag{2}$$

where $g(u\text{-}t)$ is the moving window, and the IF estimate $\omega_0(t,\omega)$ can be written as

$$\omega_0(t,\omega) = \frac{\partial_t G(t,\omega)}{iG(t,\omega)} \tag{3}$$

A harmonic signal whose expression can be written as

$$s(t) = A(t)\cdot e^{i\varphi(t)} \tag{4}$$

The IF of a harmonic signal can be considered as a constant, and the amplitude of STFT can be expressed as

$$\begin{aligned}&\left|G_h\left(t,\varphi'(t)\right)\right| \\ &= \left|\int_{-\infty}^{+\infty} e^{-i\varphi'(t)u}\cdot s(u)\cdot g(u-t)du\right| \\ &= A(u)\cdot\left|\int_{-\infty}^{+\infty} e^{-i\varphi'(t)u}\cdot e^{i\varphi(u)}\cdot g(u-t)du\right|\end{aligned}$$

$$
\begin{aligned}
&= A(u) \cdot \left| \int_{-\infty}^{+\infty} e^{i\varphi'(t)u - i\varphi'(t)u} \cdot g(u-t)du \right| \\
&= A(u) \cdot |g(u-t)du| \\
&= A(u) \cdot \hat{g}(0)
\end{aligned} \tag{5}
$$

According to [23], the model of an FM signal can be expressed as

$$
s(t) = A(t) \cdot e^{i(\varphi(t) + \varphi'(u-t)\mathrm{t} + \varphi''(t)(u-t)^2/2)} \tag{6}
$$

The amplitude of STFT of the FM signal can be written as

$$
\begin{aligned}
&\left|G_{\mathrm{m}}(t, \varphi'(t))\right| \\
&= \left| \int_{-\infty}^{+\infty} g(u-t) \cdot s(u) \cdot e^{-i\varphi'(t)u} du \right| \\
&= A(u) \cdot \left| \int_{-\infty}^{+\infty} g(u-t) \cdot e^{i(\varphi(t) + \varphi'(u-t)\mathrm{t} + \varphi''(t)(u-t)^2/2)} \right. \\
&\quad \left. \cdot e^{-i\varphi'(t)u} du \right| \\
&= A(u) \cdot \left| \int_{-\infty}^{+\infty} g(u-t) \cdot e^{i\varphi(t)} \cdot e^{i\varphi'(t)u} \cdot e^{-i\varphi'(t)t} \right. \\
&\quad \left. \cdot e^{i\varphi''(t)(u-t)^2/2} \cdot e^{-i\varphi'(t)u} du \right| \\
&= A(u) \cdot \left| \int_{-\infty}^{+\infty} g(u-t) \cdot e^{i\varphi(t)} \cdot e^{-i\varphi'(t)t} \cdot e^{i\varphi''(t)(u-t)^2/2} du \right| \\
&= A(u) \cdot \left| e^{i\varphi(t)} \cdot e^{-i\varphi'(t)t} \right| \cdot \left| \int_{-\infty}^{+\infty} g(u-t) \cdot e^{i\varphi''(t)(u-t)^2/2} du \right| \\
&= A(u) \cdot \hat{g}(r)
\end{aligned} \tag{7}
$$

Since it is an FM signal, $i\varphi''(t)(u-t)^2/2$ is not zero. The Fourier transform of the window function is the maximum value at zero, so $\hat{g}(r) < \hat{g}(0)$. By comparing (5) and (7), we can see that the amplitude of the modulated signal is lower than that of the harmonic signal, i.e., $\left|G_{\mathrm{m}}\left(t, \varphi'(t)\right)\right| < \left|G_{\mathrm{h}}\left(t, \varphi'(t)\right)\right|$. The main reason is the existence of a modulated element $e^{i\varphi''(t)(u-t)^2/2}$. Therefore, when processing the FM signal, the result of STFT smear heavily. Here, we use the numerical signal (8) in [25] for further explanation. In addition, white noise is added to the signal, and the signal-to-noise ratio (SNR) is equal to 20 dB. Fig. 1(a-b) shows the result of STFT. We can see that the energy of the FM part is blurry seriously.

$$
s(t) = \begin{cases} \sin(2\pi \cdot (25 \cdot t + 10 \cdot \sin(t))), & 0 < t \le 6 \\ \sin(2\pi \cdot 34.6 \cdot t), & 6 < t \le 14 \end{cases} \tag{8}
$$

As a post-processing tool, SST also produces the same phenomenon. As shown in Fig.1(c-d), the energy of the FM part is blurry than that of the harmonic part, which leads to the inaccurate estimation of the IF.

III. THE PROPOSED METHOD

A. PARAMETERIZED STFT

The most important step to obtain an ideal TF representation is to accurately estimate the IF of the original TFA method.

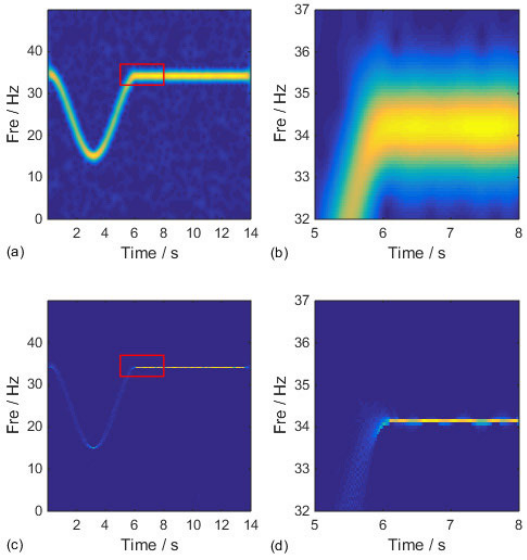

FIGURE 1. The signal (8) with the SNR is equal to 20 dB. (a) STFT result, (b) zoom of STFT result, (c) SST result, and (d) zoom of SST result.

STFT is often unable to effectively characterize the time-varying features of the FM signal, so we need to eliminate the influence of the FM part on STFT, so that the original spectrogram can effectively describe the time-varying features of strong FM signals. Therefore, we use the demodulated operator to correct the bias estimation of TF.

According to (7), we get that the modulated element $e^{i\varphi''(t)(u-t)^2/2}$ affects the STFT result. To eliminate the influence of modulated element, it is necessary to introduce a demodulated operator $e^{-i\beta(t)(u-t)^2/2}$, so we get the following formula

$$
G(t, \varphi'(t)) = \int_{-\infty}^{+\infty} g(u-t) \cdot s(u) \cdot e^{-i\varphi'(t)u} \cdot e^{-i\beta(t)(u-t)^2/2} du \tag{9}
$$

The amplitude of it can be written as

$$
\begin{aligned}
&\left|G(t, \varphi'(t))\right| \\
&= \left| \int_{-\infty}^{+\infty} g(u-t) \cdot s(u) \cdot e^{-i\varphi'(t)u} \cdot e^{-i\beta(t)(u-t)^2/2} du \right| \\
&= \left| \int_{-\infty}^{+\infty} g(u-t) \cdot A(u) \cdot e^{i(\varphi(t) + \varphi'(u-t)\mathrm{t} + \varphi''(t)(u-t)^2/2)} \right. \\
&\quad \left. \cdot e^{-i\varphi'(t)u} \cdot e^{-i\beta(t)(u-t)^2/2} du \right| \\
&= A(u) \cdot \left| \int_{-\infty}^{+\infty} e^{i(\varphi''(t) - \beta(t))(u-t)^2/2} \cdot g(u-t) du \right| \\
&\le A(u) \left| \int_{-\infty}^{+\infty} g(u-t) du \right|
\end{aligned} \tag{10}
$$

If $\varphi''(t) = \beta(t)$, the amplitude will achieve its maximum value in the IF. Actually, it is often impossible to determine the value $\beta(t)$, so we use a series of discrete β to approximate the best-demodulated operator $e^{-i\beta(t)(u-t)^2/2}$. The STFT formula for considering the discrete demodulated operator is as

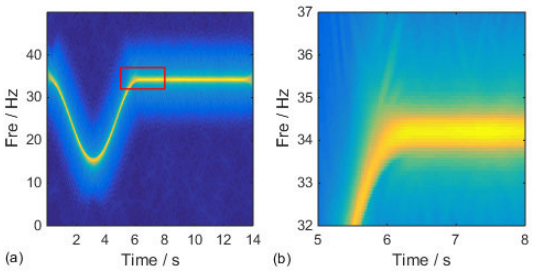

FIGURE 2. The signal (8) with the SNR is equal to 20 dB. (a) PSTFT result, and (b) zoom of PSTFT result.

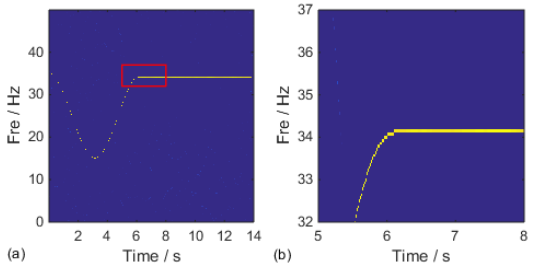

FIGURE 3. The signal (8) with the SNR is equal to 20 dB. (a) PLMSST result, and (b) zoom of PLMSST result.

follows

$$G(t,\varphi'(t),\beta)=\int_{-\infty}^{+\infty} g(u-t)\cdot s(u)\cdot e^{-i\varphi'(t)u}\cdot e^{-i\beta(t)(u-t)^2/2}du \tag{11}$$

According to [26], a rotating parameter α is introduced, which will produce a rotation effect on the TF plane, and the rotating degree is $\arctan(-\beta)$.

$$\beta=\frac{F_S}{2T_S}\tan(\alpha),\quad \alpha\in(-\pi/2,\pi/2) \tag{12}$$

where T_S is the sampling time and F_S is the sampling frequency. There are N values with α.

$$\alpha=-\frac{\pi}{2}+\frac{\pi}{N+1},-\frac{\pi}{2}+\frac{2\cdot\pi}{(N+1)},\ldots,-\frac{\pi}{2}+\frac{N\cdot\pi}{(N+1)} \tag{13}$$

In this way, we get the parameterized short-time Fourier transform (PSTFT), and its expression can be written as

$$G(t,\omega,\alpha)=\int_{-\infty}^{+\infty} g(u-t)\cdot s(u)\cdot e^{-i\omega u}\cdot e^{-i\cdot\tan(\alpha)\frac{F_S}{2T_S}(u-t)^2/2}du \tag{14}$$

Fig.2(a-b) shows the TF representation of PSTFT. We can see that the energy of the signal is concentrated at the IF and around it. At the same time, the amplitude $|G(t,\omega,\alpha)|$ reaches the maximum. In this way, we correct the deviation of TF estimation and accurately describe the time-varying features of FM signals.

B. LOCAL MAXIMUM TF REASSIGNMENT

PSTFT provides an accurate IF result, but the high-resolution TF representation cannot be obtained. SST squeezes the TF coefficients into the IF trajectory, which can improve the TF resolution, but its noise robustness is poor. Inspired by [14], we further process the PSTFT result by detecting the local maximum of the spectrogram in the frequency direction and forming a new frequency-reassignment operator.

$$\omega_m(t,\omega)=\begin{cases}\arg\max\limits_{\omega}|G(t,\omega,\alpha)|,\\ \omega\in[\omega-\Delta,\omega+\Delta], & \text{if } |G(t,\omega,\alpha)|\neq 0\\ 0, & \text{if } |G(t,\omega,\alpha)|=0\end{cases} \tag{15}$$

Assuming that two arbitrary modes are well separated at sufficient frequency distance, i.e., $\varphi'_{k+1}(t)-\varphi'_k(t)>4\Delta$. where Δ is the discrete frequency interval. The Fourier transform of the window function reaches the maximum at zero, so we can get

$$\omega_m(t,\omega)=\begin{cases}\varphi'_k(t), & \text{if } \omega\in\left[\varphi'_k(t)-\Delta,\varphi'_k(t)+\Delta\right]\\ 0, & \text{otherwise}\end{cases} \tag{16}$$

By parameterizing STFT and local maximizing TF reassignment, we obtain a new TFA method named parameterized local maximum synchrosqueezing transform (PLMSST). It can be written as

$$PLMSST(t,\omega',\alpha)=\int_{-\infty}^{+\infty} G(t,\omega,\alpha)\delta\left(\omega'-\omega_m(t,\omega)\right)d\omega \tag{17}$$

We can see that the proposed method accurately describes the time-varying features of the signal (8) (see Fig. 3(a-b)), and obtains the high-resolution TF representation, which is almost equivalent to the ideal TFA (ITFA) (see Fig. 4(a-b)).

C. SIGNAL RECONSTRUCTION

Since the TF coefficients are only reassigned in the frequency direction, the proposed method supports signal reconstruction.

By calculating the integral in the frequency direction, we get

$$\begin{aligned}&\int_{-\infty}^{+\infty} PLMSST(t,\omega',\alpha)d\omega'\\ &=\int_{-\infty}^{+\infty}\int_{-\infty}^{+\infty} G(t,\omega,\alpha)\delta\left(\omega'-\omega_m(t,\omega)\right)d\omega' d\omega\\ &=\int_{-\infty}^{+\infty} G(t,\omega,\alpha)\int_{-\infty}^{+\infty}\delta\left(\omega'-\omega_m(t,\omega)\right)d\omega' d\omega\\ &=\int_{-\infty}^{+\infty} G(t,\omega,\alpha)d\omega\\ &=2\pi g(0)s(t)\end{aligned} \tag{18}$$

Then, we can recover the original signal perfectly

$$s(t)=\frac{1}{2\pi g(0)}\int_{-\infty}^{+\infty} PLMSST(t,\omega',\alpha)d\omega \tag{19}$$

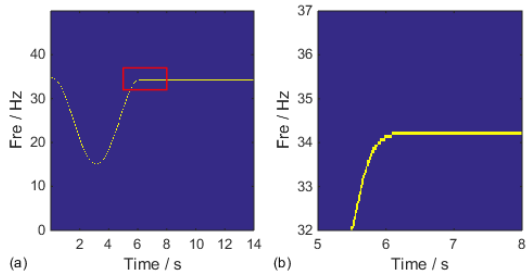

FIGURE 4. The signal (8) with the SNR is equal to 20 dB. (a) ITFA representation, and (b) zoom of ITFA representation.

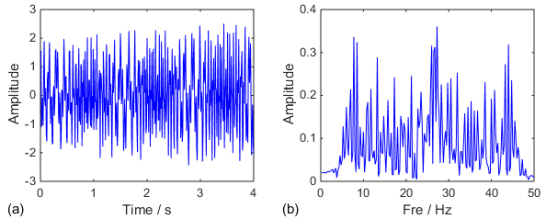

FIGURE 5. The signal (22). (a) The waveform, and (b) the spectrum.

For the multi-component modes, each mono-component mode is decomposed from the TF coefficients in the IF trajectories of the PLMSST representation, and the expression is as follows

$$s_k(t) = \frac{1}{2\pi g(0)} PLMSST\left(t, \varphi_k'(t), \alpha\right) \tag{20}$$

A popular algorithm [15], [20] of IF trajectories detection is written as

$$E(\varphi_k(t)) = \sum_{k=1}^{K} \int_{-\infty}^{+\infty} |TFR(t, \varphi_k(t))|^2 dt - \int_{-\infty}^{+\infty} \left(\lambda \cdot \varphi_k'(t)^2 + \eta \cdot \varphi_k''(t)^2\right) dt \tag{21}$$

IV. NUMERICAL VALIDATION

A. SIMULATED FM SIGNAL

In this section, we construct a simulated FM signal to illustrate the performance of PLMSST comparing with other TFA methods.

$$\begin{aligned} S_1(t) &= e^{0.05t} \sin(2\pi(35t + 2\sin(5t))) \\ S_2(t) &= e^{0.1t} \sin(2\pi(17t + 2.2\sin(5t))) \\ S(t) &= S_1(t) + S_2(t) \end{aligned} \tag{22}$$

The sampling frequency is 100 Hz and the sampling time is 4 s. The waveform and the spectrum are shown in Fig. 5 (a-b). However, it is difficult to understand the nonlinear behaviors of the signal only from the information in Fig. 5.

To obtain more information, we need to extend the time-varying features into the 2D TF plane with the help of TFA methods. The results obtained by STFT, PSTFT, SST, fourth-order SST, SET, and PLMSST are shown in Fig. 6(a-d) and Fig. 7(a-b). We can see that although the result of STFT

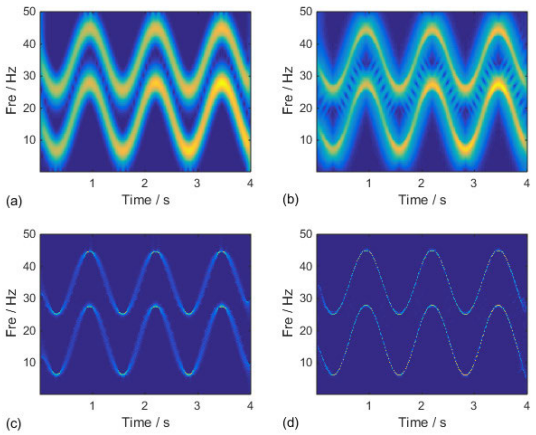

FIGURE 6. The signal (22). (a) STFT result, (b) PSTFT result, (c) SST result, and (d) fourth-order SST result.

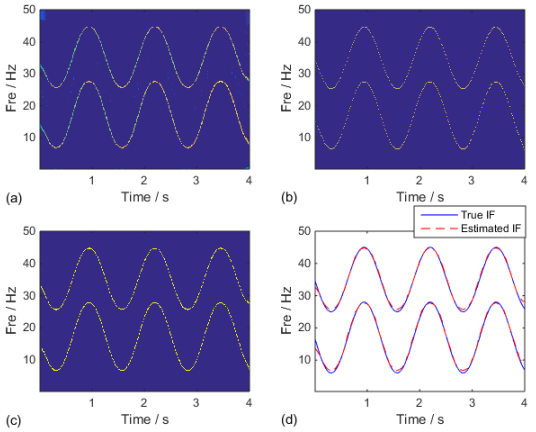

FIGURE 7. The signal (22). (a) SET result, (b) PLMSST result, (c) ITFA representation, and (d) detected IFs.

is smeared, it can basically reveal the law of frequency information changing with time. The energy of PSTFT is more concentrated at the IF and around it, which corrects the deviation of TF estimation, but does not obtain a high-resolution TF representation. Both SST and fourth-order SST show more concentrated results than that of STFT, but the phenomenon of energy distribution still exists. SET is an excellent TFA method with a concentrated TF representation. The PLMSST result shows more concentrated TF features than the other results, and approximates the ITFA representation (see Fig. 7(c)). To decompose the two modes, it is necessary to detect the IF trajectories. Due to the energy-concentrated TF result of PLMSST, the detected IF trajectories are very close to the true IF (see Fig. 7(d)).

Rényi entropy is usually used to evaluate the energy concentration of a TFA method. A lower Rényi entropy value denotes a more energy-concentrated TF representation [20]–[23]. To quantitatively evaluate the energy concentration of different TFA methods, white noises with signal-to-noise ratios (SNRs) of 1–30 dB are added to the signal. Fig. 8 shows the Rényi entropies of different TFA methods under different noise levels. We can see that among

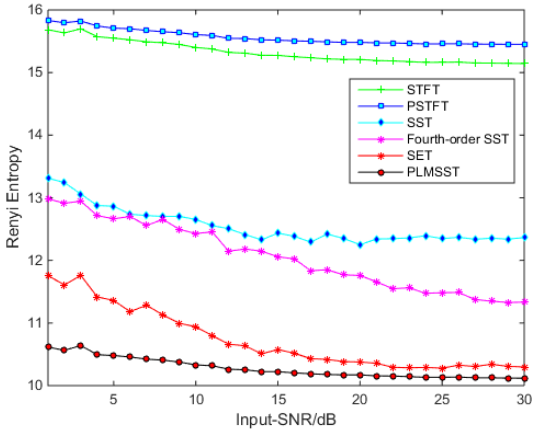

FIGURE 8. The signal (22). Under different noise levels (SNRs of 1-30 dB), the Rényi entropies of the TF representations generated by different TFA methods.

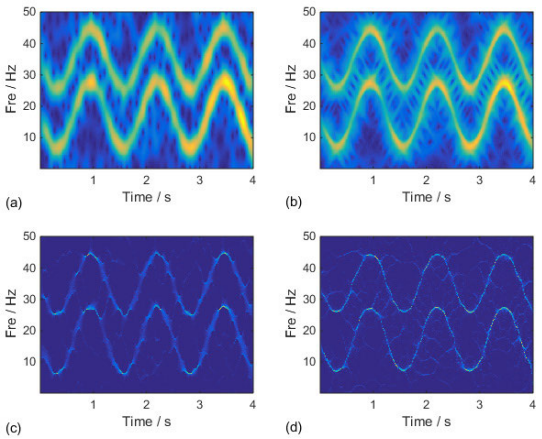

FIGURE 9. The signal (22) with the SNR is equal to 11 dB. (a) STFT result, (b) PSTFT result, (c) SST result, and (d) fourth-order SST result.

these TFA methods, the Rényi entropy of PLMSST is the smallest under each noise level, which shows that PLMSST has the best ability to generate an energy-concentrated TF representation when processing the FM signals with noise.

In addition, to explore the differences of the above TFA methods in processing noise signals, the corresponding results are listed in Fig. 9(a-d) and Fig. 10(a-b) (the SNR of the signal is equal to 11 dB). We can also see that PLMSST obtains the energy-concentrated TF representation, while other TFA methods are affected by noises at different levels. Thanks to the post-processing of PSTFT, the detected IF trajectories of the PLMSST representation are very close to the true IF (see Fig. 10(c-d)).

The IF trajectories estimated by the PLMSST result can be used to decompose the mono-component mode effectively. Two decomposed modes are shown in Fig. 11(a-b). In Fig. 11(c), we show the summation of two components. Their errors are shown in Fig. 11(d). We can see that the reconstruction errors of the proposed method are small, indicating that PLMSST has good reversibility.

It is very important for the computational efficiency of a TFA algorithm, so we test the computational time of the

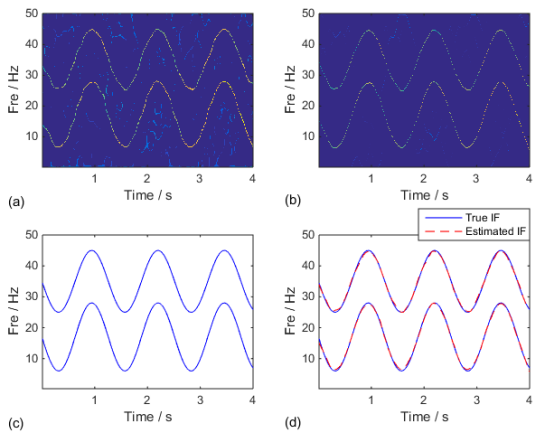

FIGURE 10. The signal (22) with the SNR is equal to 11 dB. (a) SET result, (b) PLMSST result, (c) true IFs, and (d) detected IFs.

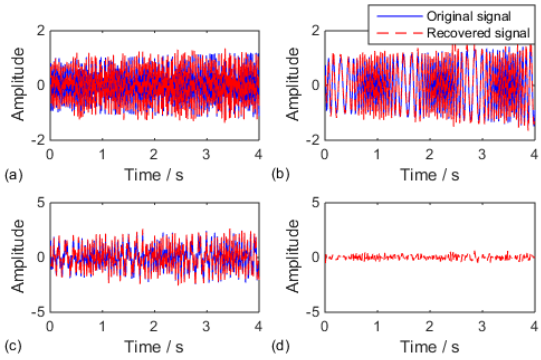

FIGURE 11. The signal (22) with the SNR is equal to 11 dB. (a) Recovered S1, (b) recovered S2, (c) recovered S, and (d) the errors between the recovered signal and the original signal.

TABLE 1. Required computational time by several TFA methods.

TFA	STFT	PSTFT	SST	4-th SST	SET	PLMSST
Time (s)	0.006	0.216	0.104	0.759	0.260	0.523

above-mentioned methods in addressing this noisy signal. The tested computer configuration is as follows: Intel Core i7-7700 3.60 GHz, 8.0 GB of RAM, and MATLAB version R2016a. The computational time of these methods are listed in Table 1. Because it takes time to detect the local maximum of the spectrogram, the calculation time of the proposed method is long, but less than the fourth-order SST method.

B. STRONGLY TIME-VARYING SIGNAL

To further verify the performance of this method in processing the strongly time-varying signal, we use a strongly time-varying signal borrowed from [17], [23] to analyze. The signal is modeled as

$$\begin{aligned} S_1(t) &= \sin(2\pi(340t - 2\exp(-2t+0.4)\sin(14\pi(t-0.2)))) \\ S_2(t) &= \sin(2\pi((75t + 30t^3))) \\ S(t) &= S_1(t) + S_2(t) \end{aligned} \tag{23}$$

The sampling frequency is 1024 Hz, and the sampling time 1s. For further comparison, here we compare with some

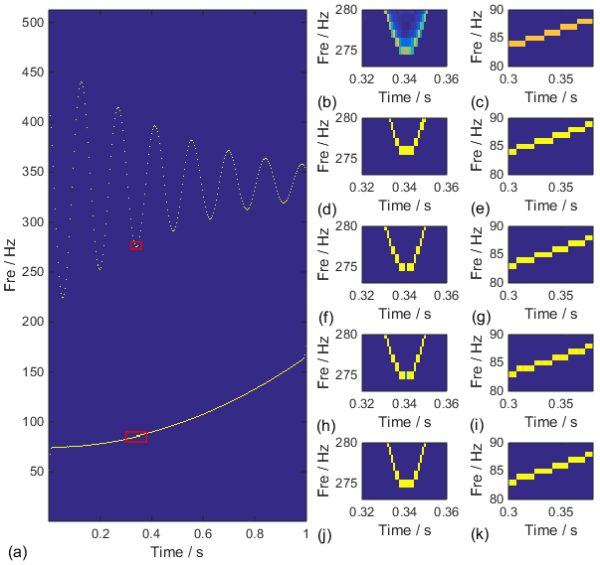

FIGURE 12. The signal (23). (a) PLMSST result, (b) zoom of fourth-order SST result, (c) zoom of fourth-order SST result, (d) zoom of SET result, (e) zoom of SET result, (f) zoom of PSE result, (g) zoom of PSE result, (h) zoom of MSSCT result, (i) zoom of MSSCT result, (j) zoom of PLMSST result, and (k) zoom of PLMSST result.

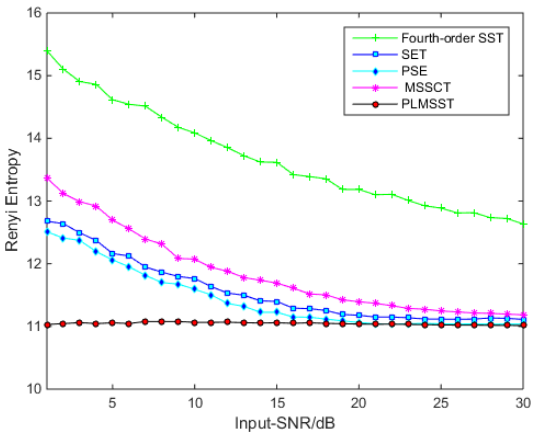

FIGURE 13. The signal (23). Under different noise levels (SNRs of 1-30 dB), the Rényi entropies of the TF representations generated by different TFA methods.

new methods like fourth-order SST and SET, and some more advanced methods such as PSE and MSSCT. The TF representations of the signal obtained by fourth-order SST, SET, PSE, MSSCT, and PLMSST are shown in Fig. 12. We can see that all these advanced TFA methods can obtain the energy-concentrated TF representation except fourth-order SST. White noises with signal-to-noise ratios (SNRs) of 1–30 dB are added to the signal.

Fig. 13 shows the Rényi entropies of different TFA methods under different noise levels. We can see that among these TFA methods, the Rényi entropy of PLMSST is the smallest under each noise level, which shows that PLMSST has the best ability to generate an energy-concentrated TF representation when processing the strong FM signal. The computational time of different TFA methods are listed in

FIGURE 14. Structural sketch of the machine set.

TABLE 2. Required computational time by several TFA methods.

TFA	4-th SST	SET	PSE	MSSCT	PLMSST
Time (s)	4.933	0.2301	1.7699	2.388	3.727

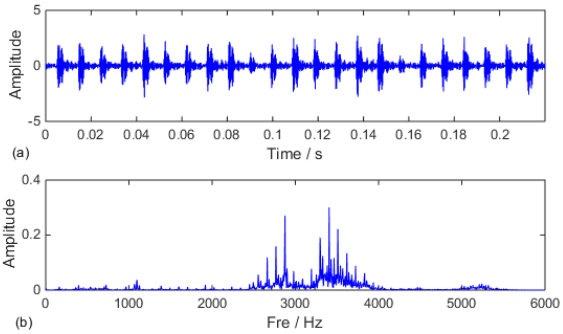

FIGURE 15. The bearing vibration signal with the outer ring fault. (a) The waveform, and (b) the spectrum.

Table 2. We can see that when processing the strong FM signals, the proposed method does not take the longest time among these methods.

V. EXPERIMENTAL VALIDATION

A. BEARING OUTER RACE FAULT VIBRATION SIGNAL

In this section, the bearing defect signal containing the outer ring fault provided by Western Reserve University Bearing Data Center [23] is analyzed to validate the proposed method. The structural sketch of the machine set is shown in Fig. 14. The test bearing is used to support the motor shaft, and the speed is 1772 r/min. The sampling frequency is 12000 Hz, and the sampling time 0.2205 s. According to the information of bearing parameters and speed, we can know that the theoretical value of fault characteristic frequency of the outer ring fault is 105.9Hz.

The time-domain waveform and the spectrum of the vibration signal are shown in Fig. 15(a) and (b), and the frequency components are mainly around 2600-3800 Hz. For better comparison, we list the TF results of STFT, SST, fourth-order SST, PLMSST, SET, PSE, and MSSCT of 0.1 s (see Fig. 16 and Fig. 17), representing the oscillated TF features of the two modes M1 and M2. We can see from Fig. 16(d) that the proposed method achieves better TF location ability and

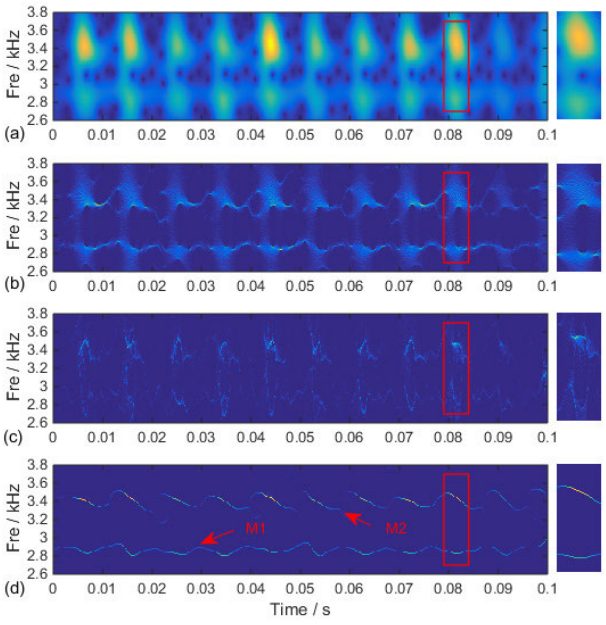

FIGURE 16. The bearing vibration signal with the outer ring fault. (a) STFT result, (b) SST result, (c) fourth-order SST, and (d) PLMSST result.

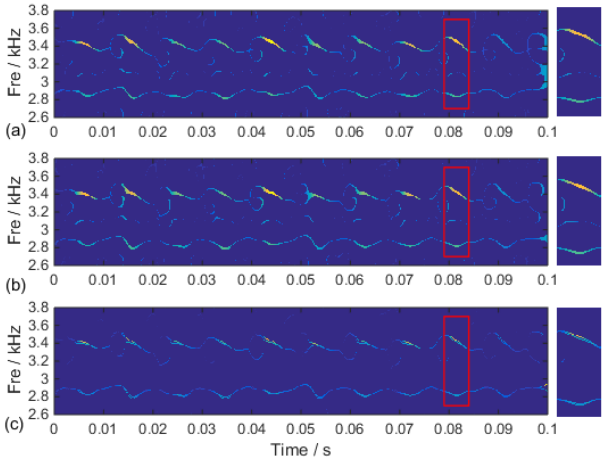

FIGURE 17. The bearing vibration signal with the outer ring fault. (a) SET result, (b) PSE result, and (c) MSSCT.

accurately characterizes the duration time and the frequency band of each transient component.

The Rényi entropies of these methods are calculated and listed in Table 3. We can see that the Rényi entropy of PLMSST is the lowest, which indicates that the proposed method can obtain the most energy-concentrated TF representation among these TFA methods. The computational time of these methods are listed in Table 4. We can see that the calculation time of all the methods is within 30 s, and the time consumption of the proposed method is 24.182 s, which is less than that of the fourth-order SST. At the same time, we detect the IF of two modes from the PLMSST result. Fig. 18(a) and (c) show the IF of M1 and its spectrum. Fig. 18(b) shows the reconstructed time-series waveform of the mode M1. We can see that the spectrum has a fault

TABLE 3. Rényi entropy.

TFA	STFT	SST	4th-order SST	PLMSST
Rényi entropy	19.2210	17.3407	16.4507	14.265
TFA	SET	PSE	MSSCT	
Rényi entropy	14.4314	14.4135	15.8192	

TABLE 4. Required computational time by several TFA methods.

TFA	STFT	SST	4th-order SST	PLMSST
Time (s)	0.162	4.147	29.568	24.182
TFA	SET	PSE	MSSCT	
Time (s)	1.25	10.246	14.6113	

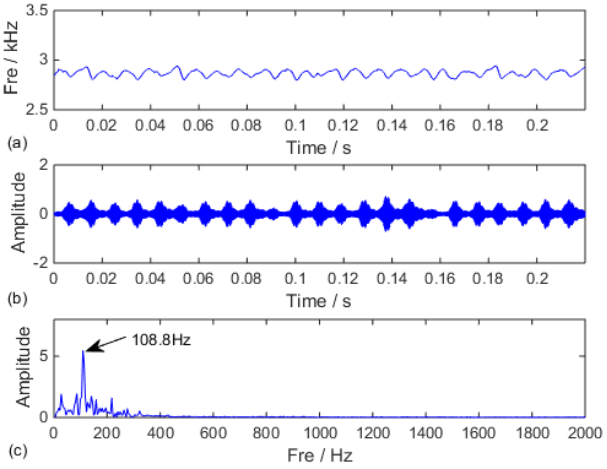

FIGURE 18. (a) Detected IF trajectory of M1, (b) recovered signal of M1, and (c) the spectrum of the detected IF trajectory of M1.

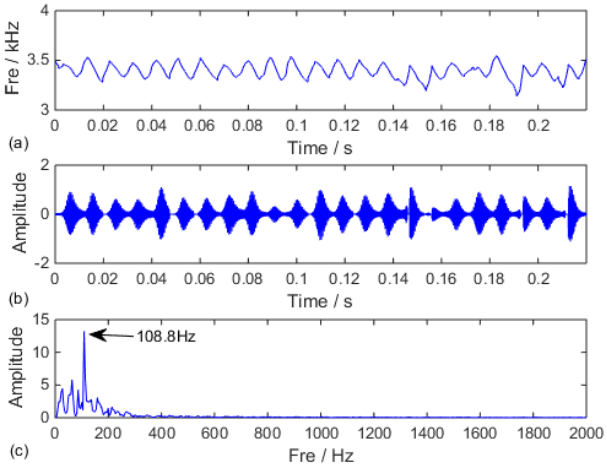

FIGURE 19. (a) Detected IF trajectory of M2, (b) recovered signal of M2, and (c) the spectrum of the detected IF trajectory of M2.

frequency of 108.8 Hz, which is very close to the theoretical fault frequency and is not found in the spectrum of the original signal (see Fig. 15(b)).

Fig. 19(a) and (c) show the IF of M2 and its spectrum. Fig. 19(b) shows the reconstructed time-series waveform of

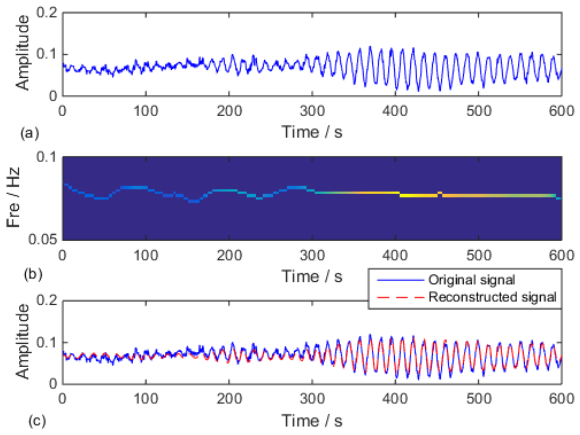

FIGURE 20. The bridge vibration signal. (a) The waveform, (b) PLMSST result, and (c) recovered signal.

TABLE 5. Rényi entropy.

TFA	STFT	SST	4th-order SST	PLMSST
Rényi entropy	17.501	13.405	13.257	12.540
TFA	SET	PSE	MSSCT	
Rényi entropy	12.845	12.767	12.878	

the mode M2. The frequency of the outer ring fault can also be found. Therefore, it can be considered that the concentrated TF representation provides a precise way for fault diagnosis based on bearing vibration signals.

B. BRIDGE VIBRATION SIGNAL

To further investigate the applicability of this method, the measured bridge vibration signal [28] is analyzed. The sampling frequency is 5 Hz and the sampling time is 600 s. Fig. 20(a) and (b) show the waveform of the signal and the TF representation of PLMSST. From the TF representation of PLMSST, it is obvious that the amplitude of the signal is low in the front half part (0-300 s) and accompanied by certain FM phenomenon. While in the latter part (300-600 s), the FM phenomenon is weakened obviously. These indicate that when the vibration amplitude of the bridge is small, the variation of the frequency may be caused by the background noise. Fig. 20 (c) shows the reconstructed signal of PLMSST. Compared with the original signal, we can see that the noise components are basically eliminated, leaving the characteristic of a relatively regular oscillation.

For further comparison, the TF representations of STFT, SST, fourth-order SST, SET, PSE, and MSSCT are listed in Fig. 21 and Fig. 22. The Rényi entropies of these methods are calculated and shown in Table 5. Both the TF representations and Rényi entropies show that the proposed has the best ability to characterize the bridge vibration signal.

C. BEARING EARLY RUB-IMPACT FAULT VIBRATION SIGNAL

In this section, the proposed method is employed to characterize the vibration signals collected from a heavy oil catalytic

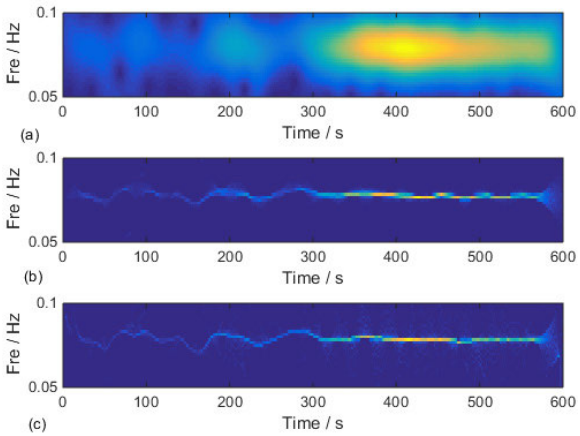

FIGURE 21. The bridge vibration signal. (a) STFT result, (b) SST result, and (c) fourth-order SST result.

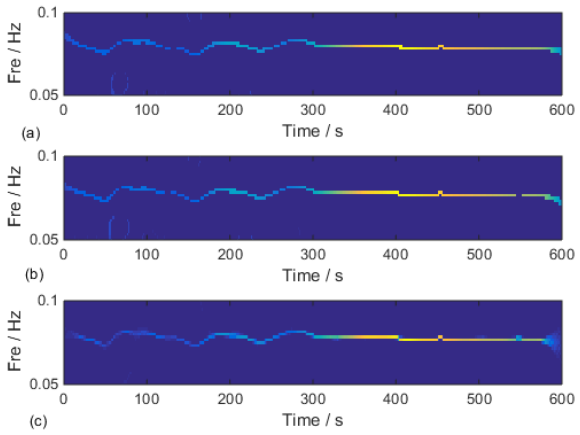

FIGURE 22. The bridge vibration signal. (a) SET result, (b) PSE result, and (c) MSSCT result.

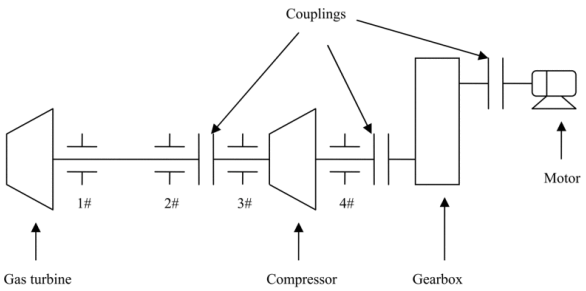

FIGURE 23. Structural sketch of the machine set.

cracking machine set with a rub-impact fault [20], [29]. The structural sketch is shown in Fig. 23. It consists of a gas turbine, compressor, gearbox, and motor. The gas turbine is used to transform heat energy to mechanical energy. The bearing cases (1#, 2#, 3#, and 4#) are used to support the corresponding shaft. The rotation speed of the gas turbo is 5381 r/min (the rotating frequency is approximately equal to 90 Hz). The vibration of bush 2 is large than the alarm limit, so we analyze the signal with the proposed method.

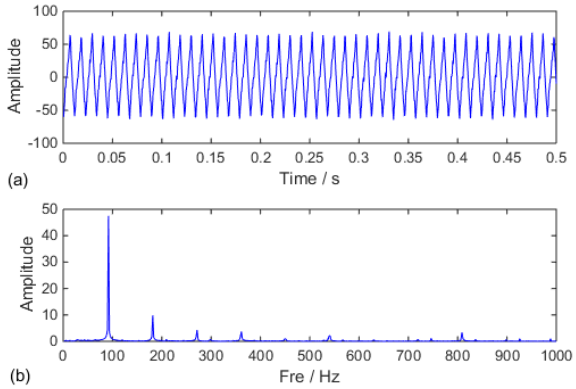

FIGURE 24. The bearing vibration signal with the rub-impact fault. (a) The waveform, and (b) the spectrum.

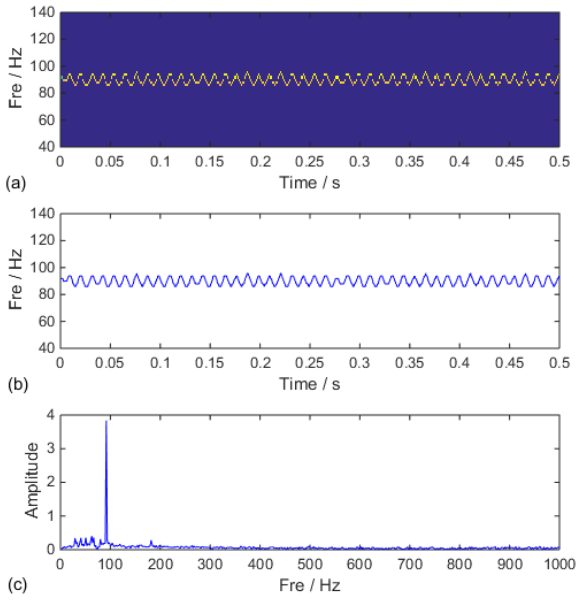

FIGURE 25. The bearing vibration signal with the rub-impact fault. (a) PLMSST result, (b) the detected IF trajectory, and (c) the spectrum of the detected IF trajectory.

The sampling frequency is 2 kHz and the sampling number is 1024. The time-domain waveform and the spectrum of the vibration signal are shown in Fig. 24(a) and (b). The first-order rotating frequency is the largest component, which corresponds to the main fault reason. PLMSST is used to analyze the vibration signal. The TF result in the frequency bank of 40-140 Hz generated by the proposed method is shown in Fig. 25(a), which clearly shows that the FM component has a periodic oscillatory IF. We detect the IF of the component from the PLMSST result. Fig. 25(b) and (c) show the detected IF trajectory and its spectrum. The result shows that the IF of mode M1 periodically oscillates around first-order rotating frequency with a frequency of 90 Hz. The reason is that the rub-impact fault makes the rotor running at an unstable speed [20], [30].

VI. CONCLUSION

In this paper, we proposed a new TFA method to characterize the features of engineering vibration signals. By parameterizing TFA and local maximizing TF reassignment, the proposed method corrects IF bias estimation caused by noise interference of FM signal and greatly improves the energy concentration of the TF result, allowing for perfect signal reconstruction. This is very beneficial to the analysis and processing of engineering vibration signals. The advantages of the proposed method were demonstrated through numerical simulation and practical applications. In addition, we focused on the comparisons of the proposed method with other classical and advanced methods. Compared with other TFA methods, the proposed method has the best performance in engineering vibration signal processing.

REFERENCES

[1] F. Auger and P. Flandrin, "Improving the readability of time-frequency and time-scale representations by the reassignment method," *IEEE Trans. Signal Process.*, vol. 43, no. 5, pp. 1068–1089, May 1995, doi: 10.1109/78.382394.

[2] I. Daubechies, J. Lu, and H.-T. Wu, "Synchrosqueezed wavelet transforms: An empirical mode decomposition-like tool," *Appl. Comput. Harmon. Anal.*, vol. 30, no. 2, pp. 243–261, Mar. 2011, doi: 10.1016/j.acha.2010.08.002.

[3] C. L. Herry, M. Frasch, A. J. Seely, and H.-T. Wu, "Heart beat classification from single-lead ECG using the synchrosqueezing transform," *Physiol. Meas.*, vol. 38, no. 2, pp. 171–187, Feb. 2017, doi: 10.1088/1361-6579/aa5070.

[4] H. Liu, K. Yang, Y. Ma, Q. Yang, and C. Huang, "Synchrosqueezing transform for geoacoustic inversion with air-gun source in the east China sea," *Appl. Acoust.*, vol. 169, Dec. 2020, Art. no. 107460, doi: 10.1016/j.apacoust.2020.107460.

[5] P. Wang, J. Gao, and Z. Wang, "Time-frequency analysis of seismic data using synchrosqueezing transform," *IEEE Geosci. Remote Sens. Lett.*, vol. 11, no. 12, pp. 2042–2044, Dec. 2014, doi: 10.1109/LGRS.2014.2317578.

[6] D. Camarena-Martinez, C. A. Perez-Ramirez, M. Valtierra-Rodriguez, J. P. Amezquita-Sanchez, and R. D. J. Romero-Troncoso, "Synchrosqueezing transform-based methodology for broken rotor bars detection in induction motors," *Measurement*, vol. 90, pp. 519–525, Aug. 2016, doi: 10.1016/j.measurement.2016.05.010.

[7] Y. Guan, M. Liang, and D.-S. Necsulescu, "Velocity synchronous linear chirplet transform," *IEEE Trans. Ind. Electron.*, vol. 66, no. 8, pp. 6270–6280, Aug. 2019, doi: 10.1109/TIE.2018.2873520.

[8] C. Li and M. Liang, "A generalized synchrosqueezing transform for enhancing signal time–frequency representation," *Signal Process.*, vol. 92, no. 9, pp. 2264–2274, Sep. 2012, doi: 10.1016/j.sigpro.2012.02.019.

[9] C. Li and M. Liang, "Time–frequency signal analysis for gearbox fault diagnosis using a generalized synchrosqueezing transform," *Mech. Syst. Signal Process.*, vol. 26, pp. 205–217, Jan. 2012, doi: 10.1016/j.ymssp.2011.07.001.

[10] Z. Feng, X. Chen, and M. Liang, "Iterative generalized synchrosqueezing transform for fault diagnosis of wind turbine planetary gearbox under nonstationary conditions," *Mech. Syst. Signal Process.*, vols. 52–53, pp. 360–375, Feb. 2015, doi: 10.1016/j.ymssp.2014.07.009.

[11] S. Wang, X. Chen, G. Cai, B. Chen, X. Li, and Z. He, "Matching demodulation transform and SynchroSqueezing in time-frequency analysis," *IEEE Trans. Signal Process.*, vol. 62, no. 1, pp. 69–84, Jan. 2014, doi: 10.1109/TSP.2013.2276393.

[12] S. Wang, X. Chen, C. Tong, and Z. Zhao, "Matching synchrosqueezing wavelet transform and application to aeroengine vibration monitoring," *IEEE Trans. Instrum. Meas.*, vol. 66, no. 2, pp. 360–372, Feb. 2017, doi: 10.1109/TIM.2016.2613359.

[13] S. Wang, X. Chen, I. W. Selesnick, Y. Guo, C. Tong, and X. Zhang, "Matching synchrosqueezing transform: A useful tool for characterizing signals with fast varying instantaneous frequency and application to machine fault diagnosis," *Mech. Syst. Signal Process.*, vol. 100, pp. 242–288, Feb. 2018, doi: 10.1016/j.ymssp.2017.07.009.

[14] G. Yu, Z. Wang, P. Zhao, and Z. Li, "Local maximum synchrosqueezing transform: An energy-concentrated time-frequency analysis tool," *Mech. Syst. Signal Process.*, vol. 117, pp. 537–552, Feb. 2019, doi: 10.1016/j.ymssp.2018.08.006.
[15] T. Oberlin, S. Meignen, and V. Perrier, "Second-order synchrosqueezing transform or invertible reassignment? Towards ideal time-frequency representations," *IEEE Trans. Signal Process.*, vol. 63, no. 5, pp. 1335–1344, Mar. 2015, doi: 10.1109/TSP.2015.2391077.
[16] R. Behera, S. Meignen, and T. Oberlin, "Theoretical analysis of the second-order synchrosqueezing transform," *Appl. Comput. Harmon. Anal.*, vol. 45, no. 2, pp. 379–404, Sep. 2018, doi: 10.1016/j.acha.2016.11.001.
[17] D.-H. Pham and S. Meignen, "High-order synchrosqueezing transform for multicomponent signals analysis—With an application to gravitational-wave signal," *IEEE Trans. Signal Process.*, vol. 65, no. 12, pp. 3168–3178, Jun. 2017, doi: 10.1109/tsp.2017.2686355.
[18] W. Liu, W. Chen, and Z. Zhang, "A novel fault diagnosis approach for rolling bearing based on high-order synchrosqueezing transform and detrended fluctuation analysis," *IEEE Access*, vol. 8, pp. 12533–12541, 2020, doi: 10.1109/ACCESS.2020.2965744.
[19] X. Tu, Y. Hu, F. Li, S. Abbas, Z. Liu, and W. Bao, "Demodulated high-order synchrosqueezing transform with application to machine fault diagnosis," *IEEE Trans. Ind. Electron.*, vol. 66, no. 4, pp. 3071–3081, Apr. 2019, doi: 10.1109/TIE.2018.2847640.
[20] G. Yu, M. Yu, and C. Xu, "Synchroextracting transform," *IEEE Trans. Ind. Electron.*, vol. 64, no. 10, pp. 8042–8054, Oct. 2017, doi: 10.1109/TIE.2017.2696503.
[21] X. Zhu, Z. Zhang, J. Gao, B. Li, Z. Li, X. Huang, and G. Wen, "Synchroextracting chirplet transform for accurate IF estimate and perfect signal reconstruction," *Digit. Signal Process.*, vol. 93, pp. 172–186, Oct. 2019, doi: 10.1016/j.dsp.2019.07.015.
[22] K. Yu, T. R. Lin, H. Ma, H. Li, and J. Zeng, "A combined polynomial chirplet transform and synchroextracting technique for analyzing nonstationary signals of rotating machinery," *IEEE Trans. Instrum. Meas.*, vol. 69, no. 4, pp. 1505–1518, Apr. 2020, doi: 10.1109/TIM.2019.2913058.
[23] G. Yu, Z. Wang, and P. Zhao, "Multisynchrosqueezing transform," *IEEE Trans. Ind. Electron.*, vol. 66, no. 7, pp. 5441–5455, Jul. 2019, doi: 10.1109/TIE.2018.2868296.
[24] X. Zhu, Z. Zhang, Z. Li, J. Gao, X. Huang, and G. Wen, "Multiple squeezes from adaptive chirplet transform," *Signal Process.*, vol. 163, pp. 26–40, Oct. 2019, doi: 10.1016/j.sigpro.2019.05.008.
[25] G. Yu, "Demodulated synchrosqueezing transform," in *Proc. Chin. Autom. Congr. (CAC)*, Xi'an, China, Nov. 2018, pp. 3468–3471, doi: 10.1109/CAC.2018.8623521.
[26] G. Yu and Y. Zhou, "General linear chirplet transform," *Mech. Syst. Signal Process.*, vols. 70–71, pp. 958–973, Mar. 2016, doi: 10.1016/j.ymssp.2015.09.004.
[27] W. A. Smith and R. B. Randall, "Rolling element bearing diagnostics using the case western reserve university data: A benchmark study," *Mech. Syst. Signal Process.*, vols. 64–65, pp. 100–131, Dec. 2015, doi: 10.1016/j.ymssp.2015.04.021.
[28] Bcyangbc, Shengzhenzhijia, China. (Nov. 8, 2009). [Online]. Available: http://forum.vibunion.com/thread-88198-1-1.html
[29] S. Wang, X. Chen, G. Li, X. Li, and Z. He, "Matching demodulation transform with application to feature extraction of rotor rub-impact fault," *IEEE Trans. Instrum. Meas.*, vol. 63, no. 5, pp. 1372–1383, May 2014, doi: 10.1109/TIM.2013.2283552.

ZHENFENG HUANG received the B.S. degree in mechanical engineering from the South China University of Technology, China, in 1984. He is currently a Professor with the School of Mechanical Engineering, Guangxi University. His research interests include advanced signal processing techniques, mechanical equipment control, electromechanical product development, nondestructive testing, and condition monitoring and fault diagnosis.

DAHUAN WEI received the B.S. degree in mechanical engineering from Guangxi University, China, in 2017, where he is currently pursuing the M.S. degree with the School of Mechanical Engineering. His research interests include advanced signal processing techniques, nondestructive testing, and condition monitoring and fault diagnosis.

ZHIWEI HUANG received the B.S. degree in mechanical engineering from Guangxi University, China, in 2018, where he is currently pursuing the M.S. degree with the School of Mechanical Engineering. His research interests include advanced signal processing techniques, nondestructive testing, and condition monitoring and fault diagnosis.

HANLING MAO received the Ph.D. degree in mechanical engineering from Zhejiang University, China, in 1995. He is currently a Professor with the School of Mechanical Engineering, Guangxi University. His research interests include mechanical equipment control, condition monitoring and fault diagnosis, nondestructive testing, and mechatronics.

XINXIN LI received the Ph.D. degree in mechanical engineering from Zhejiang University, China, in 2008. He is currently an Associate Professor with the School of Mechanical Engineering, Guangxi University. His research interests include mechanical and electronic product design, intelligent material application, vibration energy collection, and condition monitoring and fault diagnosis.

RUI HUANG received the B.S. degree in mechanical engineering from the Inner Mongolia University of Technology, China, in 2018. He is currently pursuing the M.S. degree with the School of Mechanical Engineering, Guangxi University. His research interests include advanced signal processing techniques, data mining, and computer applications.

PENGWEI XU received the B.S. degree in mechanical engineering from the Henan University of Science and Technology, China, in 2017. He is currently pursuing the M.S. degree with the School of Mechanical Engineering, Guangxi University. His research interests include rotor system dynamics, multi-objective optimization, and signal processing techniques.